



Joint Probabilistic Data Association and Smoothing Applied to Multiple Space Object Tracking

Jason Stauch*

Applied Defense Solutions, Albuquerque, New Mexico 87117

Travis Bessell[†] and Mark Rutten[‡]

Defence Science and Technology Group, Edinburgh, South Australia 5111, Australia

Jason Baldwin[§]

Air Force Research Laboratory, Albuquerque, New Mexico 87117

Moriba Jah[¶]

The University of Texas, Austin, Texas 78712

and

Keric Hill^{**}

Pacific Defense Solutions (IAI), Kihei, Hawaii 96753

DOI: 10.2514/1.G002230

A foundational aspect of space domain awareness is the ability to identify and track space objects, including space object discovery and custody. This paper demonstrates the power of combining an efficient multiple hypothesis joint probabilistic data association (MH-JPDA) algorithm with a fixed-interval smoother to simultaneously track multiple space objects. For newly discovered objects, statistical initial orbit determination (SIOD) is possible with a single short optical tracklet, but results in large initial uncertainties. Combining these uncertainties with closely spaced objects can result in highly ambiguous data associations, which can lead to poor state estimates and even filter divergence. This paper invokes MH-JPDA to probabilistically update multiple tracks with multiple simultaneous observations in a sequential filter, while avoiding assigning one-to-one associations. Once sufficient information has been collected, the space objects become uniquely distinguishable among each other. Subsequently, the smoother is applied to achieve improved association of the prior observations. MH-JPDA allows for immediate track formation (using SIOD) and sequential processing of incoming observations, providing statistically rigorous real-time state estimates, whereas smoothing produces a more-refined, higher-confidence overall track estimate at user-defined intervals. This paper demonstrates this approach within the Constrained Admissible Region, Multiple Hypothesis Filter (CAR-MHF) software by tracking a simulated break-up scenario.

I. Introduction

SPACE situational awareness (SSA) is the knowledge required to detect, predict, avoid, operate through, recover from, and/or attribute cause to the loss or degradation of space activities [1]. Robust tracking capabilities are critical to forming a solid body of knowledge and understanding in the SSA domain. Foundational to this understanding is the ability to detect a high percentage of all objects, to initiate realistic and predictive trajectories (tracks) for the objects, and to maintain custody of those objects.^{††} The following is a short list of the

most significant challenges faced in achieving this understanding, and will be addressed in this paper:

- 1) Observation-to-observation (in particular UCT-to-UCT, i.e., uncorrelated tracklets), and track-to-track correlation
- 2) Angles-only (e.g., optical), short-arc statistical initial orbit determination (SIOD)
- 3) False associations, created by
 - a) Simultaneously tracking multiple objects (some of which may not have been previously tracked) with overlapping uncertainties
 - b) Fixed-gate data association, potentially combined with poor state estimates
 - c) Angles-only, short-arc SIOD methods introduce necessarily large uncertainties
 - d) Large uncertainties, combined with many closely spaced objects, exacerbates the data association problem
- 4) Need for SIOD given a single observation, along with a subsequent real-time tracking capability

We apply an efficient implementation of multiple hypothesis joint probabilistic data association (PDA) to mitigate the UCT problem, allowing immediate track formation and sequential processing to provide real-time state estimates of many previously untracked objects. Further, we apply a fixed-interval smoother to disambiguate associations and refine the state estimates.

When examining optical sensors, which provide only angle information, the problem of UCTs (i.e., a detection that cannot be combined with one or more additional detections to recover an actual object's trajectory) results from a combination of factors. Detections of new objects (i.e., measurements of objects not previously known) are typically serendipitous detections resulting from surveys or ancillary detections from images of tasked object tracking. As a result, the tracklet lengths are typically minutes or less and thus provide very limited information content with regard to space object

Received 15 May 2016; revision received 9 July 2017; accepted for publication 1 November 2017; published online 11 December 2017. Copyright © 2017 by the American Institute of Aeronautics and Astronautics, Inc. The U.S. Government has a royalty-free license to exercise all rights under the copyright claimed herein for Governmental purposes. All other rights are reserved by the copyright owner. All requests for copying and permission to reprint should be submitted to CCC at www.copyright.com; employ the ISSN 0731-5090 (print) or 1533-3884 (online) to initiate your request. See also AIAA Rights and Permissions www.aiaa.org/randp.

*Aerospace Research Engineer.

[†]Research Scientist.

[‡]Senior Research Scientist, Third Ave.

[§]Senior Research Aerospace Engineer, Space Vehicles Directorate, 3550 Aberdeen Ave. SE, Kirtland AFB.

[¶]Associate Professor, Aerospace Engineering and Engineering Mechanics Department, Cockrell School of Engineering, 210 E. 24th St. Associate Fellow AIAA.

**Senior Scientist, 535 Lipoa Pkwy, Suite 101.

^{††}Track custody here is defined as the knowledge required to positively identify and know where the space object is located at any time, to within a user-defined level of accuracy.

states and parameters, in particular for geosynchronous Earth orbit (GEO) objects.^{‡‡} Traditional initial orbit determination (IOD) methods or a batch processor requires several time-separated measurements to be correlated together. A large number of UCTs, which generally originate from many different unknown objects, create a combinatorics problem. In many cases, the inability to reliably associate data to candidate objects results in data being discarded [2,3].

Given a single, very short arc of optical data, traditional IOD methods (such as Laplace’s method [4], Gauss’s method [4], double r integration [4], or Gooding’s method [5], which are deterministic in nature and do not account for stochasticity in the measurements) tend to break down because the curvature of the arc (i.e., trajectory observability) is well within the measurement noise. These may produce an orbit estimate (of questionable quality), but any quantifiable uncertainty of the orbit is, at best, a guess. Furthermore, most of these techniques are fraught with singularities and sensitivity to the observation geometry, in addition to observation data quality (noise and biases). They do not account for nongravitational forces (e.g., solar radiation pressure) in their initial determination and subsequent propagation in order to associate future measurements.

The challenges of very short arc optical IOD, and subsequently UCT mitigation, have motivated development of the Constrained Admissible Region, Multiple Hypothesis Filter (CAR-MHF) [6,7]. The CAR-MHF algorithms exploit the information found in a single optical tracklet (set of three or more measurements within a short time, e.g., seconds or minutes, of each other), along with hypothesized assumptions, to produce statistical IOD (SIOD) information, which includes data-appropriate uncertainties. Additionally, varying area-to-mass ratio (AMR) values are hypothesized, and later refined with additional observations, to account for drag and/or solar pressure forces. This SIOD process results in a grid of hypothesized estimates, which are statistically refined with the unscented Kalman filter (UKF)-based MHF.

Large initial uncertainties, whether assumed (e.g., by the SIOD methodology) or derived (e.g., from the measurement noise), will usually result in measurement-to-track association ambiguity in a dense observation field, that is, multiple measurements at a given time being statistically likely to have originated from a given object and vice versa. This problem is amplified by closely spaced objects and/or long propagation times due to the sparse nature of UCTs. A nearest neighbor approach [8] makes one-to-one measurement-to-track assignments based on the likelihood that each measurement originates from the objects. This approach can break down for large state uncertainties and/or measurements of clustered objects, causing false associations that can lead to filter divergence. Alternatively, PDA techniques, developed and well-studied by the radar and sonar community since the 1970s [9], refine knowledge of an object’s state based on weighted information from *all* candidate measurements within the data association gate (in our case, the gate is a covariance-based region of validity). An efficient multiple hypothesis joint probabilistic data association algorithm (MH-JPDA) is incorporated into CAR-MHF to address the challenges of the multitarget-multisensor nature of space object tracking. Other multitarget tracking approaches that could be applied to this problem include multiple hypothesis tracking (MHT) [10,11] and random finite set (RFS) algorithms [12–14]; however, these are not considered here.

Although JPDA enables real-time, sequential processing in the presence of ambiguous data association, addition of a backward smoother can help disambiguate the associations. Smoothing refines the state at each measurement time based upon the information content of all the measurements obtained over an interval of time—in this respect it is similar to a batch processor (or differential correction). This refinement improves association performance, in particular at the time of the large initial uncertainties described above. The improved associations further refine the trajectory estimate. A previously developed Rauch, Tung, Striebel (RTS, i.e., fixed-interval) smoother for the UKF [15–17] is incorporated into

CAR-MHF to enable this association and tracking enhancement. Moreover, “tentative” (forward-filtered only) tracks that pass a series of convergence and smoother consistency checks (e.g., McReynolds consistency [18]) are graduated to “established” (smoothed) tracks, which, one can be confident, contain correct (often one-to-one) associations and thus reliable state and uncertainty estimates.

The contribution of this work is the unique combination of the above techniques that have been extensively implemented in the air/maritime (and others) tracking community (i.e., MHF, JPDA, and smoothing) and the asteroid tracking community (i.e., CAR) and the application to the space domain within the context of CAR-MHF. Specifically, the proposed method accomplishes initial orbit determination and follow-on tracking, taking into account probability of detection less than one, with embedded multi-observation/multi-target data association, and taking into account background object/measurement clutter statistics. These concepts have not previously been combined in such a way, and further, although prior application of JPDA, in particular, has enjoyed success in other domains with unknown dynamics and high measurement rate scenarios, this presentation demonstrates enhancement of the method to be useful in fairly well-known dynamics environments with relatively sparse observations. Although this work was motivated by the UCT problem, the methods extend to other challenges in space object tracking, for example, data association with sparse measurements (i.e., long propagations) and/or closely spaced objects (e.g., clusters). In Sec. II, a background of the major elements of CAR-MHF is reviewed. Sections III and IV provide the MH-JPDA and RTS UKF smoother algorithms. Finally, Sec. V presents the results of processing simulated observations of a geosynchronous satellite break-up scenario.

II. CAR-MHF Background

As an SIOD and tracking strategy, CAR-MHF combines the statistical track initialization capability of the CAR (Sec. II.A) with an MHF (Sec. II.B) that implements an UKF to associate future measurements to the newly initialized track and refine the trajectory and uncertainties.

Previous work analyzed the ability of CAR-MHF to perform SIOD and subsequently track high AMR (HAMR) debris objects over a 2-week span using PDA for the data association [19]. For that analysis, CAR-MHF processed all objects simultaneously; however, the object dispersion did not dictate the need for JPDA (joint PDA only becomes necessary when measurement(s) fall within the uncertainty gate of multiple objects). Nevertheless, these results demonstrate the ability of CAR-MHF to correctly estimate object states covering a range of orbit and AMR values.

Previous work also analyzed the performance of CAR-MHF with respect to a low Earth orbit break-up event [20]. It was found that CAR-MHF could initialize and characterize the orbit and drag states in an accurate, unambiguous, and autonomous fashion. Though the data association produced favorable results for this limited data set (only 10 fragments were considered; again, JPDA was not necessary), it was suggested that in a more cluttered data environment other techniques would need to be applied.

The remainder of this section provides an overview of the main components of CAR-MHF. A detailed description of JPDA and smoothing is deferred to the subsequent sections.

A. Constrained Admissible Region (CAR)

As the name suggests, the CAR involves constraining the possible ambiguity space of a short tracklet (set of three or more measurements within a short time, e.g., seconds or minutes, of each other) of optical data to an admissible region, following the method presented by Milani et al. [21]. Figure 1 illustrates how the CAR is used to form 6-D state hypotheses given a set of 2-D measurements. In the upper left, a tracklet of optical data is compressed (see Sec. II.D) to form a single 4-D angles and angle-rates measurement ($\alpha, \delta, \dot{\alpha}, \dot{\delta}$, blue circle at top middle) and associated uncertainty (based on the raw measurement noise). As shown by DeMars and Jah [7], this measurement is used to derive semi-major axis (SMA) and eccentricity (e) constraints in

^{‡‡}GEO is defined as the orbital region where the mean motion of a space object is equivalent to a sidereal day, approximately 24 h.

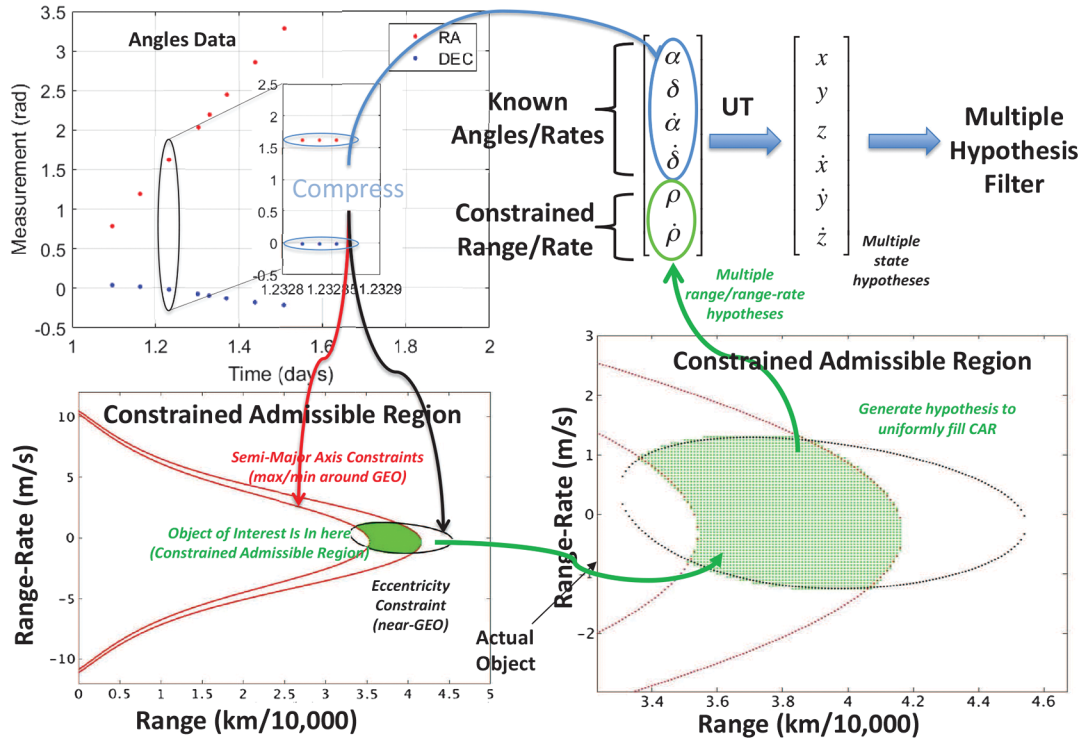


Fig. 1 Illustration of the CAR being used to produce a multiple hypothesis SIOD.

range/range-rate space (lower right, red parabolic and black elliptical lines, respectively), creating a CAR (the intersection of the SMA and e constraints, represented in green in the two lower plots). A grid is formed within the CAR to form a set of $(\rho, \dot{\rho})$ hypotheses (green circle at top middle), with an assumed uncertainty of uniform distribution based on the density of hypotheses. This yields a set of hypotheses in observation space $(\alpha, \delta, \dot{\alpha}, \dot{\delta}, \rho, \dot{\rho})$ with associated covariance (the covariance is formed from the compressed measurement noise and range/range-rate distribution spacing). An unscented transform [22] is used to transform the measurement-space hypotheses mean/covariance into Cartesian state-space $(x, y, z, \dot{x}, \dot{y}, \dot{z})$, top middle) that can readily form the a priori means and covariances to initiate the MHF.

B. Multiple Hypothesis Filter (MHF)

The MHF used in CAR-MHF follows the method introduced by DeMars et al. [6]. This should not be confused with a multiple hypothesis tracker (MHT [8,23]), which hypothesizes all possible data association combinations over some interval of time (i.e., it is not a sequential, real-time tracker). Figure 2 illustrates one recursion of

the MHF. In the MHF (which is a sequential processor), the estimated state of an object is represented by multiple Gaussian state hypotheses (upper left). Each hypothesis is propagated (upper right) and updated (lower left) using the UKF algorithm in Table 1. Additionally, each hypothesis has a respective weighting term. All hypotheses are initialized by CAR with equal weights summing to 1. During the update step, the weight of each hypothesis is updated based on the likelihood that the observation originated from that hypothesis. The weights are held constant during the propagation step (a constraint that was later relaxed by DeMars et al. with AEGIS in a Gaussian Mixture Model filter [24]). After each update, if the weight of a given hypothesis is below some threshold, the hypothesis is pruned (lower right), allowing for the MHF to eventually converge to a single hypothesis (or in some cases, a small set of statistically similar hypotheses).

As mentioned, the MHF uses the UKF, a special case of the sigma-point Kalman filter [25] that employs the unscented transform [22]. The full, nonlinear equations of motion and measurement-state equations are used. Background on the UKF is found in the references above, and additionally, van der Merwe provides an excellent source for variations and algorithms [26]. Note that the UKF in the MHF presented by DeMars et al. is the scaled UKF. CAR-MHF uses an unscaled UKF. We have found that, in processing real space object data, the lack of tuning parameters in the unscaled UKF makes this method more attractive and has yielded improved results and robustness. Given the ample literature on the UKF, only a brief summary of the unscaled UKF is given in Table 1. Notes on Table 1: \hat{x}_k^- and P_k^- are the a priori estimated state and covariance at time k ; \hat{x}_k^+ and P_k^+ are the a posteriori estimated state and covariance at time k ; S is defined as the square root (Cholesky decomposition) of the covariance and s_i are the columns of S ; n_x is the number of state elements; \mathcal{X}_i and \mathcal{Y}_i are the i th state-space sigma point (SP) and measurement-space SP (i.e., state-space SP transformed into measurement-space), respectively; w is the (evenly distributed) SP weight; $f()$ and $h()$ are the dynamic model and measurement model, respectively; Q_k and R are the process noise and measurement noise, respectively; $\hat{y}_k, P_{yy,k}, P_{xy,k}$, and K_k are the computed measurement, innovations covariance, state-measurement cross-covariance, and Kalman gain at time k , respectively; and y_k and v_k are the measurement and innovation at time k .

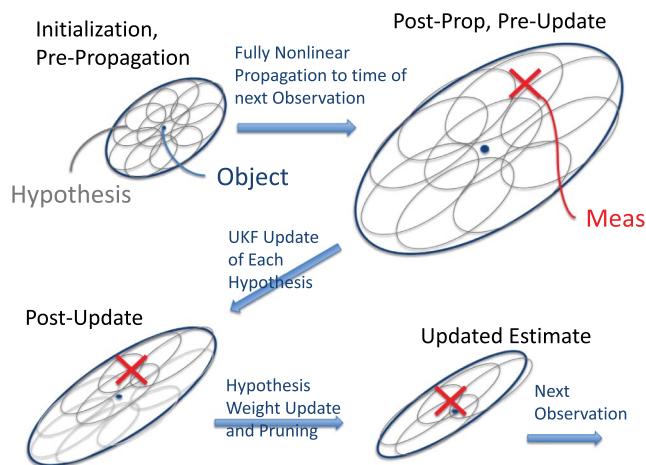


Fig. 2 Illustration of one recursion of the MHF.

Table 1 The unscaled UKF algorithm

Propagation step (predictive)	Update step (corrective)
$S_{k-1} = \text{Cholesky}(P_{k-1}^+)$	$\mathcal{Y}_{i,k} = \mathbf{h}(\mathcal{X}_{i,k}^-, t)$
$\mathcal{X}_{i,k-1}^+ = \hat{\mathbf{x}}_{k-1}^+ \pm \sqrt{n_x} s_{i,k-1}$	$\hat{\mathbf{y}}_k = \sum_{i=1}^{2n_x} w_i \mathcal{Y}_{i,k}$
where $S = [s_1, s_2, \dots, s_{n_x}]$	$P_{yy,k} = \sum_{i=1}^{2n_x} w_i (\mathcal{Y}_{i,k} - \hat{\mathbf{y}}_k)(\mathcal{Y}_{i,k} - \hat{\mathbf{y}}_k)^T + \mathbf{R}$
$w = \frac{1}{2n_x}$	$P_{xy,k} = \sum_{i=1}^{2n_x} w_i (\mathcal{X}_{i,k}^- - \hat{\mathbf{x}}_k^-)(\mathcal{Y}_{i,k} - \hat{\mathbf{y}}_k)^T$
$\mathcal{X}_{i,k}^- \leftarrow \dot{\mathcal{X}}_i = f(\mathcal{X}_{i,k-1}^+, t)$	$\mathbf{K}_k = P_{xy,k} P_{yy,k}^{-1}$
$\hat{\mathbf{x}}_k^- = \sum_{i=1}^{2n_x} w_i \mathcal{X}_{i,k}^-$	$\boldsymbol{\nu}_k = \mathbf{y}_k - \hat{\mathbf{y}}_k$
$P_k^- = \sum_{i=1}^{2n_x} w_i (\mathcal{X}_{i,k}^- - \hat{\mathbf{x}}_k^-)(\mathcal{X}_{i,k}^- - \hat{\mathbf{x}}_k^-)^T + \mathbf{Q}_k$	$\hat{\mathbf{x}}_k^+ = \hat{\mathbf{x}}_k^- + \mathbf{K}_k \boldsymbol{\nu}_k$
	$P_k^+ = P_k^- - \mathbf{K}_k P_{yy,k} \mathbf{K}_k^T$

C. Covariance-Based Data Association

DeMars et al. [6] describe how a generalized Euclidian distance, known as the Mahalanobis distance, given by Eq. (1), is used to form a covariance-based data association (CBDA) gate in order to determine whether or not a measurement should be used to update a given estimate.

$$k^2 = (\mathbf{y} - \hat{\mathbf{y}})^T (\mathbf{P}_{yy})^{-1} (\mathbf{y} - \hat{\mathbf{y}}) \quad (1)$$

k^2 is a random variable distributed according to a chi-square distribution (valid for distributions that are sufficiently Gaussian) from which the probability that the measurement in question, \mathbf{y} , spawned from the estimated track with expected measurement, $\hat{\mathbf{y}}$, and innovations covariance, \mathbf{P}_{yy} (consistent with notation in Table 1). This is compared against a user-specified confidence interval (i.e., distance “gate”) for the purpose of data association determination.

Fixed-gate association, currently used in many operational environments in the space object tracking community, does not take into account the state estimate’s uncertainty; rather, if a measurement is within some fixed distance (in measurement space) of the predicted track state, it is assumed to be associated with that track. Provided that the covariance is representative of the actual estimation errors, CBDA is superior to a fixed-gate association in that initially uncertainty (and thus error) in an estimate could be much larger than some fixed gate, while after several updates, the uncertainty could be much smaller than the same fixed gate. Figure 3 demonstrates how a fixed gate can lead to missing associations in the former case (i.e., if the uncertainty is large and the measurement falls outside of the fixed gate, meas 1) and

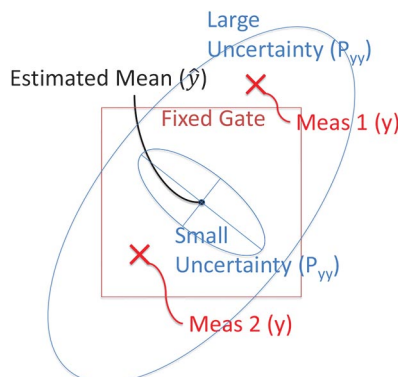


Fig. 3 Illustration of covariance-based data association, as opposed to fixed-gate data association.

and lead to false associations in the latter case (i.e., if the uncertainty is small and the measurement falls outside the covariance-based gate, but inside the fixed gate, meas 2). It is noted that although the fixed gate in the figure is rectangular, this need not be the case.

When an object’s state is represented by multiple hypotheses, the authors considered applying covariance-based data association in two ways: 1) form an overall mean and covariance based on all of the hypotheses [see Eqs. (22) and (23)] in order to form an association gate, or 2) form an association gate for each hypothesis, and if a measurement falls within any association gate, all hypotheses are updated with that measurement. The disadvantage of the former method is that if the hypotheses represent a significantly non-Gaussian distribution, the overall mean and covariance (which, by definition, represent a Gaussian distribution) may yield an association gate that is not representative of the set of hypotheses. The disadvantage of the latter method is that if a measurement falls within the gate of only one low-weighted hypothesis, it is still assumed to be associated with the object. CAR-MHF uses the latter method because given the large uncertainties of SIOD tracks, the overall track estimate can quickly become non-Gaussian (the individual hypotheses can also become non-Gaussian in time, but not at nearly the rate at which the overall track, which is typically made up of 100s or 1000s of hypotheses, does).

D. Optical Measurement Compression

In general, optical observations are collected in tracklets, a series of three or more closely spaced angles measurements. Correct observation-to-observation association (OTOA) is assumed at the tracklet level given that most sensors correctly tag observations together over these short time-scales (i.e. several seconds). Intra-tracklet associations over longer time spans (i.e. several minutes, hours or longer) are addressed as described in Sec. II.B. A transformation of variables (ToV) approach [27] is used to transform a sequence of multiple angles-only measurement pairs $(\alpha_1, \delta_1, \alpha_2, \delta_2, \dots, \alpha_n, \delta_n)$ into a single angles/angle-rates measurement quadruplet $(\alpha, \delta, \dot{\alpha}, \dot{\delta})$. This ToV approach is shown to be equivalent to passing the angles measurements through a batch processor to form the angles/angle-rates measurement. It is important to note that the compressed measurement must be formed at the midpoint (in time) of the tracklet in order to yield a diagonal measurement noise covariance. Additionally, tracklets are chosen to ensure that there is no overlap in the measurements used between compressed measurements. The advantages to measurement compression are threefold: 1) it is necessary for the CAR method used by CAR-MHF, 2) it reduces the number of observations to filter within the MHF, and 3) angle-rate information doubles the number of dimensions for covariance-based data association (i.e., more information is used to make PDA decisions).

III. Joint Probabilistic Data Association Filter (JPDAF)

The topic of multitarget-multisensor tracking has been studied by the radar and sonar communities (among others) since the 1970s. One of the most studied and used methods is a class of techniques called PDA, which we have chosen to implement because it is a proven multitarget data association technique, with advantages in tracking closely spaced objects when compared with single-object methods. Bar-Shalom and Li provide a text with a thorough development of these techniques [9]. When multiple objects exist (or when returns from a source other than the object of interest are detected, i.e., clutter⁸⁸), the situation in which multiple, simultaneous observations associate with a single (or multiple) object(s) must be considered. PDA was developed to handle tracking a single object in a cluttered environment [28] (see Fig. 4a). The probability that each observation was originated by the object of interest is computed and used in a filter (PDAF) to perform a weighted update to all of the observations (as opposed to a nearest neighbor technique, which would perform a full update to only the “closest,” or most likely, observation).

JPDA extends PDA to the situation in which multiple objects are of interest [29] (see Fig. 4b). The following development follows that of Bar-Shalom [30] (note that a more detailed development is given by Bar-Shalom and Li [9]).

A. Single Hypothesis JPDAF

First, marginal events are defined, $\theta_{r,i}$, in which observation i originates from object r , noting that $r = 0$ if measurement i originates from clutter. The set of all possible marginal events depicted in Fig. 4b is $\theta_{0,1}$ (measurement 1 originated from clutter), $\theta_{0,2}$ (measurement 2 originated from clutter), $\theta_{1,1}$ (measurement 1 originated from object 1), $\theta_{1,2}$ (measurement 2 originated from object 1), and $\theta_{2,2}$ (measurement 2 originated from object 2). $\theta_{2,1}$ is not a possible marginal event because measurement 1 is not associated with object 2. Then, a joint association event, Θ_k , is defined for each possible set of simultaneous marginal events given the association gates, where k is the index of a unique set and Θ (without subscript) is the set of all joint association events. For Fig. 4b, the set of feasible joint association events is given in Table 2, showing the assignment of measurement i to object r for each joint event.

There are two slightly different JPDA implementations: parametric and nonparametric JPDA. Stauch et al. [31] previously implemented nonparametric JPDA; however, for this application, the parametric version of JPDA is used [9]. This assumes that the sensor performance can be characterized through the probability of detection for each object, $P_{D,r}$, and the spatial density of false alarms (for the surveillance volume of the sensor), λ , in addition to the measurement noise. λ is a tuning parameter depending on the false alarm rate, which is chosen to reflect the performance of the sensor (e.g., sensor artifacts and detection processing technique). Under these assumptions the number of false alarms is implicitly Poisson distributed. This formulation offers several advantages over nonparametric JPDA:

1) The nonparametric algorithm relies on estimating the rate of false alarms from the number of measurements in the association gates. This is unreliable for sensors with very low numbers of false alarms, such as the optical systems typically used in GEO SSA.

2) The parametric version allows the algorithm designer to encode their knowledge of sensor performance via λ . Even with very little or no knowledge, one can make an educated guess by analyzing the data (similar to deriving the measurement noise of an unknown sensor).

3) The parametric derivation decouples a joint association event from the number of objects contributing to the event. This allows the association probabilities to be calculated for each object, rather than for each hypothesis of each object, resulting in dramatically reduced computational requirements [32].

⁸⁸Clutter detections generally originate from sensor artifacts (e.g., a hot pixel or cosmic ray) or detection processing. In the case of optical tracking of space objects, these types of detections are generally removed during construction of the observations, and thus clutter is typically the result of previously untracked objects (i.e., UCTs), even though these are not technically clutter.

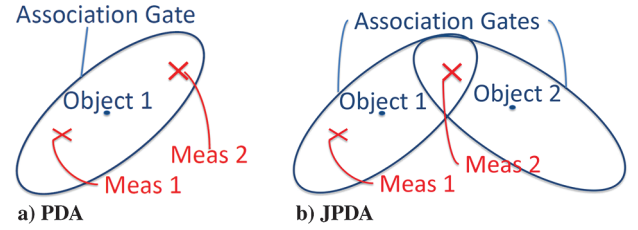


Fig. 4 Illustration of covariance-based association gate(s) for a single (left) or two (right) object(s), shown with two measurements of uncertain origin that associate with one or both objects.

The probability of a joint association event, Θ_k , given all measurements Y , is given, up to a constant of proportionality, by [9]:

$$Pr\{\Theta_k|Y\} \propto \prod_{r=1}^N \psi_{r,i_r} \quad (2)$$

where N is the total number of objects, i_r is the measurement associated with object r under Θ_k , and $\psi_{r,i}$ is the likelihood of measurement i being associated with object r :

$$\psi_{r,i} = \begin{cases} P_{D,r} \lambda^{-1} \mathcal{N}(y_i; \hat{y}_r, P_{yy,r}) & \text{for } i > 0 \\ 1 - P_{D,r} & \text{for } i = 0 \end{cases} \quad (3)$$

where y_i , \hat{y}_r , and $P_{yy,r}$ are measurement i , the expected measurement of object r , and the innovations covariance of object r , respectively (as defined in Table 1), and $\mathcal{N}()$ is described below. As a clarification of notation, for a given Θ_k the measurement/object pairings are unique, and thus an index, i_r , is defined to represent the measurement from object r within Θ_k (with corresponding marginal event θ_{r,i_r} , as an example, in Table 2, which represents Fig. 4b, for joint event Θ_3 , $i_1 = 2$ and $i_2 = 0$ and for joint event Θ_5 , $i_1 = 1$ and $i_2 = 2$). The operator $\mathcal{N}(x; \hat{x}, P)$ is the Gaussian likelihood of instantiation x given a Gaussian distribution with mean \hat{x} and covariance P :

$$\mathcal{N}(x; \hat{x}, P) = \frac{1}{\sqrt{2\pi|P|}} \exp\left(-\frac{1}{2}[x - \hat{x}]^T P^{-1}[x - \hat{x}]\right) \quad (4)$$

Then, the marginal probability that measurement i originated from object r is simply the sum of all the probabilities of the joint events in Θ that contain that marginal event, $\theta_{r,i}$:

$$\beta_{i,r} = \sum_{\Theta_k: \theta_{r,i} \in \Theta_k} Pr\{\Theta_k|Y\} \quad (5)$$

The UKF update found in Table 1 is modified to form a JPDA filter (JPDAF). Rather than computing the innovation, ν , based on a single observation (see Table 1), a JPDA-based weighted innovation (ν_r) is formed based on the innovations from all simultaneously associated observations ($\nu_{i,r} = y_i - \hat{y}_r$):

$$\nu_r = \sum_{i=1}^m \beta_{i,r} \nu_{i,r} \quad (6)$$

where m is the number of observations. Then, the state and covariance update equations for the JPDAF become

$$\hat{x}_r^+ = \hat{x}_r^- + K_r \nu_r \quad (7)$$

$$P_r^+ = P_r^- - \left(\sum_{i=1}^m \beta_{i,r} \right) K_r P_{yy,r} K_r^T + \tilde{P} \quad (8)$$

where \tilde{P} is the covariance inflation parameter that accounts for the spread of the observations:

$$\tilde{P} = K_r \left[\sum_{i=1}^m (\beta_{i,r} \nu_{i,r} \nu_{i,r}^T) - (\nu_r \nu_r^T) \right] K_r^T \quad (9)$$

Table 2 Feasible joint association events for Fig. 4b

Joint event	Marginal events	Object No. associated with measurement		Event description
		1	2	
Θ_1	$\theta_{0,1}, \theta_{0,2}$	0	0	Meas. 1 & 2 from clutter
Θ_2	$\theta_{1,1}, \theta_{0,2}$	1	0	Meas. 1 from Obj. 1, Meas. 2 from clutter
Θ_3	$\theta_{0,1}, \theta_{1,2}$	0	1	Meas. 1 from clutter, Meas. 2 from Obj. 1
Θ_4	$\theta_{0,1}, \theta_{2,2}$	0	2	Meas. 1 from clutter, Meas. 2 from Obj. 2
Θ_5	$\theta_{1,1}, \theta_{2,2}$	1	2	Meas. 1 from Obj. 1, Meas. 2 from Obj. 2

B. Multiple Hypothesis JPDAF (MH-JPDAF)

Given that CAR-MHF represents each object with multiple hypotheses, JPDA must be extended to account for multiple hypotheses (see Fig. 5 for a cartoon depicting a situation in which MH-JPDA applies). The hypothesis weighting update for the MHF is the same as that of the Interacting Multiple Model (IMM) [9] and so Chen and Tugnait's [33] development of the IMM-JPDAF is used as a basis for an MH-JPDAF. The rearrangement of IMM-JPDAF presented by Rutten et al. [32] is followed in this section.

Using the a priori weight of hypothesis j from object r , $\mu_{r,j}^-$, the contribution of each object to the joint association event Θ_k , is given by

$$\psi_{r,i} = \sum_{j=1}^{n_r} \psi_{r,i,j} \quad (10)$$

where the number of hypotheses in object r is n_r and $\psi_{r,i,j}$ is the likelihood of measurement i being associated with hypothesis j of object r :

$$\psi_{r,i,j} = \mu_{r,j}^- \times \begin{cases} P_{D,r} \lambda^{-1} \mathcal{N}(\mathbf{y}_i; \hat{\mathbf{y}}_r, \mathbf{P}_{yy,r}) & \text{for } i > 0 \\ 1 - P_{D,r} & \text{for } i = 0 \end{cases} \quad (11)$$

By using Eq. (10) [rather than Eq. (3)] in Eq. (2), the calculation of the joint event probabilities, Θ_k and the marginal probabilities, $\beta_{i,r}$, can proceed as above. In contrast with the formulation in Stauch et al. [31] and Chen and Tugnait [33], these association calculations reduce to the single hypothesis case, avoiding the expensive evaluation of joint association events for all combinations of objects, measurements, and hypotheses.

The updated hypothesis weights can then be written in terms of the association probabilities and measurement likelihoods [32], giving

$$\mu_{r,j}^+ = \sum_{i=0}^m \frac{\beta_{i,r}}{\psi_{r,i}} \psi_{r,i,j} \quad (12)$$

Similarly, the marginal probability that measurement i originates from hypothesis j of object r is

$$\beta_{i,r,j} = \frac{\beta_{i,r} \psi_{r,i,j}}{\psi_{r,i} \mu_{r,j}^+} \quad (13)$$

Replacing Eq. (6), the MH-JPDA-based weighted innovation for hypothesis j of object r is

$$\nu_{r,j} = \sum_{i=1}^m \beta_{i,r,j} \nu_{i,r,j} \quad (14)$$

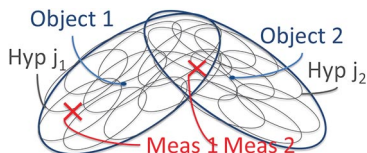


Fig. 5 Illustration of covariance-based association gates for two objects, each represented by multiple hypotheses (with respective association gates), shown with two measurements of uncertain origin that associate with one or both objects.

The state and covariance updates are the same as Eqs. (7) and (8), with hypothesis subscripts added (each hypothesis of each object is updated individually):

$$\hat{\mathbf{x}}_{r,j}^+ = \hat{\mathbf{x}}_{r,j}^- + \mathbf{K}_{r,j} \nu_{r,j} \quad (15)$$

$$\mathbf{P}_{r,j}^+ = \mathbf{P}_{r,j}^- - \left(\sum_{i=1}^m \beta_{i,r,j} \right) \mathbf{K}_{r,j} \mathbf{P}_{yy,r,j} \mathbf{K}_{r,j}^T + \tilde{\mathbf{P}} \quad (16)$$

where $\tilde{\mathbf{P}}$ is the covariance inflation parameter that accounts for the spread of the observations:

$$\tilde{\mathbf{P}} = \mathbf{K}_{r,j} \left[\sum_{i=1}^m \left(\beta_{i,r,j} \nu_{i,r,j} \nu_{i,r,j}^T \right) - \left(\nu_{r,j} \nu_{r,j}^T \right) \right] \mathbf{K}_{r,j}^T \quad (17)$$

Even after reducing the calculations to the single hypothesis case, the complexity of the joint association probability calculations still grows exponentially with the number of objects and number of measurements. Approximations can be applied to overcome this computational burden, including the use of belief propagation [34]. Additionally, the issues of track coalescence and switching are well-known and recent research suggests methods for mitigating these effects [35].

IV. Rauch-Tung-Striebel (RTS) UKF Smoother

Incorporating a smoother into a sequential filter has multiple advantages: 1) adding a smoother to a sequential filter yields similar results as a batch processor (but affording the benefits of the real-time application of a sequential filter), and 2) the smoothed solution can be used to re-initialize a forward filter, providing an initial condition with far smaller uncertainties than the SIOD-based uncertainties, improving data association performance, which results in fewer false associations and thus a better estimate of the object's state. Figure 6 illustrates how the large uncertainty associated with SIOD could result in association ambiguity, while the smoother can resolve the associations. In the forward pass, there is association ambiguity (both measurements are associated with the track), whereas in the backward smoother pass, the association ambiguity is resolved.

The RTS smoother [15], a fixed-interval smoother, was extended to the UKF by Psiaki and Wada [16] and Sarkka [17]. Working backward in time, starting at the final measurement of a given object, the RTS UKF smoother recursively computes corrections to the forward filtering result. The algorithm is summarized here. During the forward filter pass (see Table 1), the a priori and a posteriori means, $\hat{\mathbf{x}}^-$ and $\hat{\mathbf{x}}^+$, and covariances, \mathbf{P}^- and \mathbf{P}^+ , as well as the propagated sigma points (without process noise applied), \mathcal{X}^- , are saved. The smoother is initialized at the final time step of the filter, $t = T$: $\hat{\mathbf{x}}_T^* = \hat{\mathbf{x}}_T^+$ and $\mathbf{P}_T^* = \mathbf{P}_T^+$, where the * indicates the smoothed value. The following smoothing algorithm is carried out recursively from $k = T - 1$ to $k = 1$. First, the a posteriori sigma points at $t = k$, \mathcal{X}_k^+ , are computed from $\hat{\mathbf{x}}_k^+$ and \mathbf{P}_k^+ via the Cholesky decomposition (as in Table 1). Then, the cross-covariance between $t = k$ and $t = k + 1$ is computed:

$$\mathbf{C}_{k+1} = \sum_{i=1}^{2n_x} w_i (\mathcal{X}_{i,k}^+ - \hat{\mathbf{x}}_k^+) (\mathcal{X}_{i,k+1}^- - \hat{\mathbf{x}}_{k+1}^-)^T \quad (18)$$

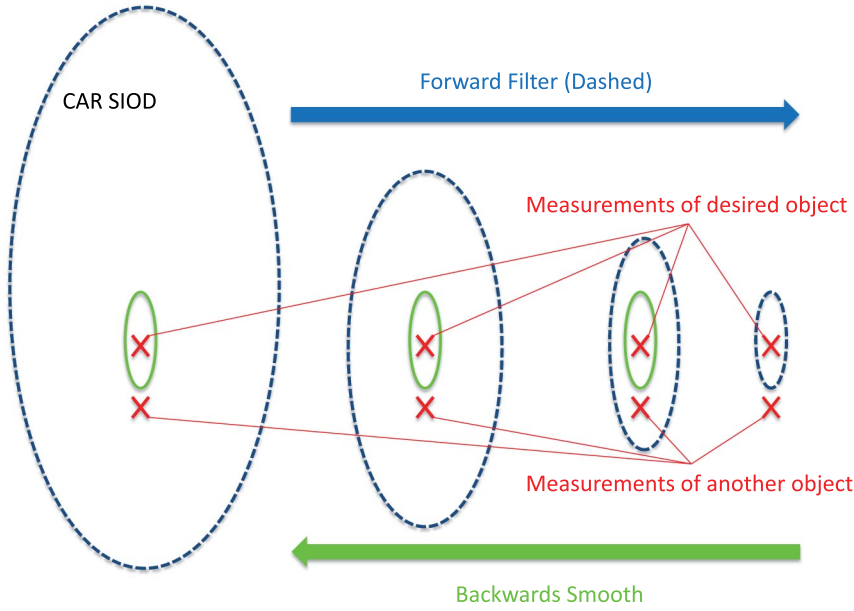


Fig. 6 Illustration of data association improvement enabled by smoothing.

where n_x is the number of state elements per hypothesis (as in Table 1). From which the smoother gain is computed:

$$\mathbf{A}_k = \mathbf{C}_{k+1}(\mathbf{P}_{k+1}^-)^{-1} \quad (19)$$

Then, the smoothed state and covariance are found as a correction to the a posteriori state and covariance from the filter pass:

$$\mathbf{x}_k^* = \hat{\mathbf{x}}_k^+ + \mathbf{A}_k(\mathbf{x}_{k+1}^* - \hat{\mathbf{x}}_{k+1}^-) \quad (20)$$

$$\mathbf{P}_k^* = \mathbf{P}_k^+ + \mathbf{A}_k(\mathbf{P}_{k+1}^* - \mathbf{P}_{k+1}^-)\mathbf{A}_k^T \quad (21)$$

We have developed a simple method to apply an RTS UKF smoother to an MH-JPDF. Each surviving hypothesis at the end of a CAR-MHF (MH-JPDF) pass is smoothed independently. Then, given the smoothed state and covariance of each hypothesis at the beginning of the data fit span, and assuming that the hypothesis weights are the same as the final a posteriori hypothesis weights, a single, merged smoothed state and covariance is computed:

$$\mathbf{x}_1^* = \sum_{j=1}^{2n} \mu_j \mathbf{x}_{j,1}^* \quad (22)$$

$$\mathbf{P}_1^* = \sum_{j=1}^{2n} \mu_j (\mathbf{P}_{j,1}^* + (\mathbf{x}_{j,1}^* - \mathbf{x}_1^*)(\mathbf{x}_{j,1}^* - \mathbf{x}_1^*)^T) \quad (23)$$

where n is the total number of surviving hypotheses at the end of the filter pass, μ_j is the final a posteriori weight of hypothesis j , and $\mathbf{x}_{j,1}^*$ and $\mathbf{P}_{j,1}^*$ are the smoothed state and covariance of hypothesis j at $t = 1$.

This merged, smoothed state and covariance is used to re-initialize a forward filter, noting that the MHF is no longer necessary because the hypotheses have been merged into a single estimate. The filter/smoothener is then iterated until filter/smoothener consistency is achieved (see below). This iterative technique allows for a restarting of the filter with another, more refined set of initial conditions, although a set informed by the data, which is akin to a batch processor being run iteratively until the initial conditions stop changing. To prevent strong cross-correlations in the smoothed covariance from enforcing undue constraints on the state elements during subsequent filter passes, only the diagonal terms are kept. Further, in order to avoid data overutilization concerns with an iterative filter/smoothener approach, the uncertainties from the smoothed covariance are multiplied by 3 in order to form the next filter iteration's a priori covariance.

Within the CAR-MHF smoother construct, filter convergence and filter/smoothener consistency are defined. In CAR-MHF, a track is deemed to be converged if the magnitude of the a posteriori position uncertainty is less than a user-defined threshold. The more converged a given track is, false associations (which degrade the estimated state) become less likely. Thus, if the estimate is converged, the smoother is invoked; otherwise, it is not. The McReynolds's filter/smoothener consistency check [18] is used to determine whether an object's smoothed solution meets the accepted criteria. McReynolds shows that variance and correlations of the difference between the filter state and the smoother state are equal to the difference between the filter covariance and smoother covariance. Thus, to find the McReynolds consistency, R , first calculate the differenced state and covariance:

$$\Delta \mathbf{x}_k = \hat{\mathbf{x}}_k^+ - \mathbf{x}_k^* \quad (24)$$

$$\Delta \mathbf{P}_k = \mathbf{P}_k^+ - \mathbf{P}_k^* \quad (25)$$

Then, the i th element of $\Delta \mathbf{x}_k$ and the square root of the i th diagonal element of $\Delta \mathbf{P}_k$, σ_k^i , are used to compute R_i (i.e., the McReynolds consistency of the i th state element):

$$R_k^i = \frac{\Delta x_k^i}{\sigma_k^i} \quad (26)$$

If the McReynolds's consistency is poor (e.g., $R_k^i \geq 3$), it is a strong indicator of poor modeling (e.g., falsely associated data or dynamic mismodeling, such as AMR). Because of the large initial ambiguity associated with the SIOD initialization, false associations are common during the first filter pass, and furthermore, there are typically large differences between the smoothed state and the SIOD-initialized state. Because of this, the filter/smoothener must be iterated two or more times to achieve consistency. If consistency is achieved within a specified number of filter/smoothener iterations, the track graduates from a "tentative" track to an "established" track and is carried forward for further measurement processing. If convergence or consistency is not achieved, the smoothed track is discarded, and the original CAR-MHF ("tentative") track (may be multiple hypotheses) is carried forward until future measurements allow for convergence and consistency.

An additional advantage to this smoother implementation is that high confidence can be placed on the data associations of established tracks. In addition to carrying these smoothed, established tracks forward, all of the observations associated with them (one-to-one,

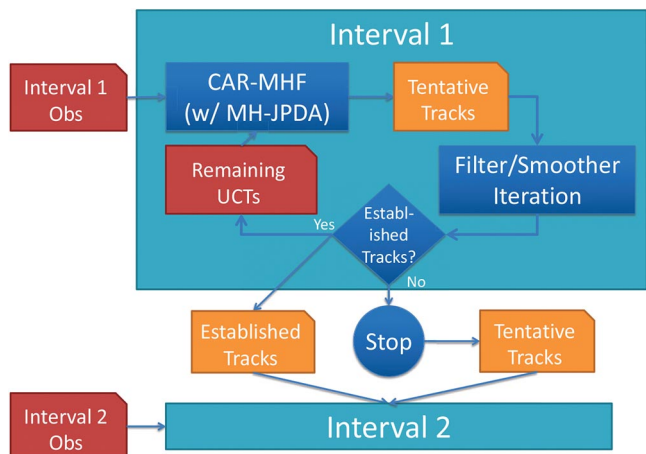


Fig. 7 Diagram of the iterative process including CAR-MHF, the filter/smother, graduation of established tracks, and pass forward to the next data interval.

unambiguous associations) are removed from the pool of UCTs, leaving a smaller pool that can be re-processed with CAR-MHF (including JPDA) and passed through another filter/smother iteration. During this next iteration, the reduction in observations can result in less confusion, which can enable graduation of additional established tracks.

Figure 7 shows a diagram of the process described above. CAR-MHF with MH-JPDA is used to process observations from (user-defined) interval 1. The resulting tentative tracks undergo a filter/smother iteration, after which tracks that pass the convergence/consistency tests graduate to established tracks and are passed forward. The remaining UCTs (after the observations associated with established tracks are removed) re-initialize CAR-MHF. This loop is continued until no more established tracks are identified, at which point the remaining tentative tracks from CAR-MHF are passed forward.

V. Example Application of CAR-MHF with MH-JPDA and Smother to a GEO Break-up Scenario

A breakup event of a geostationary (GEO) satellite is considered. Optical observations of the breakup event are simulated using a high-fidelity model. These observations are processed with CAR-MHF and the results are presented here.

A. Observation Simulation

A satellite in geostationary orbit (GEO) with 2784 kg mass is modeled as a box-wing with the satellite x axis aligned with the velocity vector and the satellite z axis constrained to point toward nadir. The cube-shaped bus has sides of 10.77 m^2 area, with three of the faces coated with Kapton and the other three coated with aluminum. Two solar arrays each with an area of 34.5 m^2 are articulated about the satellite y axis to point as closely as possible to the Sun. At 0400 hrs UTC (coordinated universal time) on February 25, 2014, the geostationary satellite vanishes and 100 fragments are formed, each with a normally distributed, random separation velocity with a standard deviation of 2 m/s in each velocity component. Although this velocity dispersion may be small compared to an actual breakup event, the low separation velocities represent a challenge for closely-spaced object data association and thus help demonstrate the innovative performance of CAR-MHF techniques. Larger separation velocities would create more of a challenge for sensor tasking, but that is outside the scope of this work. Each piece is modeled as two perpendicular flat plates with an area between roughly 2 and 5 m^2 and mass between 1 and 25 kg . The pieces are spinning with random spin axes and rates between roughly 1 and $10,000 \text{ s}$ per revolution. Orbits are propagated using a 4th/5th-order variable-step Runge Kutta integrator using a 21×21 Earth Gravitational Model (EGM) 2008 gravity field, solar and lunar gravity, and bidirectional reflectance distribution function (BRDF)—consistent solar radiation

pressure [36]. Earth's shadow is modeled using an umbra/penumbra dual-cone. The positions of the Sun and Moon are interpolated from the Jet Propulsion Laboratory (JPL) DE 421 ephemeris.

A generic optical sensor with a square field-of-view width of 2.84 deg was located in New Mexico. Starting at 0300 hrs UTC on February 25, 2014, the sensor executed a search pattern 3 fields wide and 3 fields tall centered on the expected location of the geostationary satellite. Each collection consisted of 8 exposures 1 s apart. The sensor waited approximately 1 min between collections so that the 3×3 search takes 10 min to perform. The search pattern is continuously updated to be centered on the predicted position of the GEO satellite. The sensor continues collecting observations in the search pattern for February 25, 26, and 27. The astrometric noise on the right ascension (α) and declination (δ) angles is independent and identically distributed from a normal distribution with zero mean and 2 -arcs standard deviation. The α noise is then scaled by $1/\cos(\delta)$ to account for the spherical coordinate system.

The simulated data have some noteworthy assumptions: The probability of detection is assumed to be 1 (i.e., if the fragment is in the sensor's field of view, an observation is generated). In reality, the debris pieces would be of varying size and shape and would have differing observability. Some fragments would only be observable from time to time (i.e., glints), if at all. Pixel blending is also not considered. Initially, the fragments would be close enough together to be unresolvable by the sensor (i.e., they occupy the same pixel, or neighboring pixels, creating a "blob," rather than unique observations).

B. CAR-MHF Processing

The dynamic model used for the UKF in CAR-MHF uses the following: Pines representation [37] of a 12×12 EGM-96 spherical harmonic Earth gravity field, Sun, and Moon gravitational forces (using JPL Mice Ephemerides to compute the Sun and Moon positions), and a simple spherical-object solar radiation pressure model. Process noise is applied as an acceleration uncertainty to account for dynamic mismodeling ($5e-7$, $5e-7$, and $5e-8 \text{ m/s}^2$ in the radial, intrack, and crosstrack directions, respectively). A Gaussian measurement noise of 2 arc-s in α and δ is applied. The smoother convergence criterion was set to 500 m and the maximum allowable McReynolds consistency for strong candidates was set to 3 . The position, velocity, and $C_r A/m$ (coefficient of reflectivity times AMR) are estimated.

Three scenarios were considered: 1) process observations of 25 randomly chosen fragments, starting at breakup $+4 \text{ h}$; 2) process observations of 50 randomly chosen fragments, starting at breakup $+4 \text{ h}$; and 3) process observations of all 100 fragments, starting at breakup $+1 \text{ day}$. To avoid the very tight cluster immediately after breakup, the first 4 h of data after the breakup are ignored. Theoretically, the MH-JPDA technique is capable of successfully processing such tight clustering; however, current computational limitations (both memory and processor) prohibit practical demonstration in this scenario. Note that even after breakup $+4 \text{ h}$, considerable association ambiguity exists and the merits of the MH-JPDA implementation are demonstrated in the results. Additionally, as mentioned in the previous subsection, in practice, sensor resolution would prohibit distinct object observations until the objects drifted apart to some extent.

For brevity, only results from the 25-fragment scenario are presented in detail. Over the time span of the run, $34,011$ observations of the 25 fragments are generated. Each tracklet is compressed, resulting in 3954 compressed observations (composed of between 7 and 16 observations each). Each fragment generated at least 120 tracklets over the 3-day span, with most generating nearly 150 . CAR-MHF autonomously processes these observations sequentially. Any existing tracks are propagated to the time of the next observation (or set of simultaneous observations), if the observation(s) associates (using CBDA, Sec. II.C) with any existing tracks, those tracks are updated (using MH-JPDA, if necessary, Sec. III.A). If the observation(s) does not associate with any existing tracks, new tentative tracks are spawned using CAR (Sec. II.A).

At the end of the data span, tentative tracks that are converged are smoothed back over the data time span. Given the large initial ambiguities associated with the CAR SIOD process, the McReynolds consistency is not checked for the first filter/smoothen iteration. The smoothed states are used to re-initialize the a priori state of each converged track to be processed by the MH-JPDAF (note that each smoothed track is now represented by a single hypothesis). Again, any converged tracks are smoothed. The McReynolds consistency of each track is computed, and if $R < 3$ over all the data, the tentative track is promoted to an established track, and all of the observations that are strongly associated (i.e., $\beta > 0.99$, indicating one-to-one, or very nearly one-to-one, assignments) with the fragment are removed from the observations pool. The filter/smoothen iteration is repeated until 1) all tentative tracks are promoted to established, or 2) a user-defined maximum iterations is reached.

At this point, some number of established tracks have been generated and the associated observations have been removed from the pool of observations. Then, CAR-MHF processes only the remaining observations (UCTs). Given the smaller set of observations, false associations are less likely, and thus tracks that were tainted by false associations during the first CAR-MHF run may be promoted during the second run. Again, the filter/smoothen iteration is executed. If more established tracks are identified, the associated observations are removed from the pool and CAR-MHF is run again on the remaining observations. This process is repeated until established tracks are no longer identified.

C. Results

As mentioned previously, only the detailed results of the 25-fragment case are presented, but a summary of the 25-, 50- and 100-fragment runs is given in Table 3. A total of 50 established tracks were formed in the 50-fragment case and 99 established tracks were formed in the 100-fragment case. The particular fragment missed in the 100-fragment case was an extremely high area-to-mass ratio (HAMR) object. These objects prove difficult to maintain custody of as they are highly affected by solar radiation pressure, and thus require high-fidelity modeling and accurate characterization. CAR-MHF has the impressive ability to maintain custody of HAMR objects [19] and demonstrated this ability in the 50-fragment scenario (which contained this same HAMR object). However, in the 100-fragment scenario, which started on day 2 instead of day 1, there was not sufficient temporal separation in the measurements to adequately estimate the AMR, and thus the tentative track was unable to pass convergence/consistency checks. The number of false tracks is also noteworthy (this is derived from the number of tentative tracks minus the number of fragments in the run), especially in the 50-fragment run. This is because when considering 50 fragments, there is still a large amount of confusion at breakup +4 h, which causes relatively poor MH-JPDA performance that takes some time to overcome, and thus many false tracks are created. Even so, the smoothen process is able to track all 50 fragments. The average RMS errors are derived from the difference between the estimated trajectories and the truth. More discussion is found in Sec. V.C.3.

The results of the 25-fragment scenario are evaluated in several ways:

1. Evaluation of measurement-to-track association performance
2. Analysis of filter/smoothen outputs for each established track individually (e.g., state uncertainties, a priori and a posteriori residuals, and McReynold's consistency)
3. Comparison of the estimated track states with the truth states

The upshot of method 2, and method 1 to some extent, is that the evaluation is made in the absence of truth data. Each of the three methods of evaluation is shown here.

1. Evaluation of Association Performance

CAR-MHF ignores the object ID tags in the data, but rather uses CBDA (see Sec. II.C), and MH-JPDA (Sec. III.A), where necessary, to assign measurement-to-track associations. These assignments by CAR-MHF can be evaluated against the true object IDs that generated the measurements. Given the nature of JPDA, the idea of association is no longer definitive. A single track can associate to several simultaneous measurements, and a single measurement might associate with multiple tracks. The parameter β [i.e., the marginal probability that an observation originated from a track; see Eqs. (5) and (13)] identifies the “strength” of the association. If $\beta \approx 1$, the association is strong; if $\beta \approx 0$, the association is weak.

It is interesting to evaluate the results of both the tentative tracks generated during the initial pass through the data using CAR-MHF with MH-JPDA and then compare it to the performance of established tracks that are promoted during the filter/smoothen iteration. Table 4 shows the association performance of both the initial CAR-MHF (filtered-only) tentative tracks and the smoothed established tracks. Columns 1 and 2 are the object ID and the (true) number of compressed observations of the fragment. Column 3 is the assigned number of the tentative track that corresponds to the object ID from column 1 (this number is assigned at “birth”; thus, the first track spawned by CAR is track #1, the second is track #2, and so on, and thus the order is not necessarily consistent with the object ID, but rather which fragment happened to be detected first). This correspondence between tentative track number and object ID was identified in postprocessing: if the final five observations associated with a tentative track were tagged with the same object ID, then that track was judged as corresponding with the fragment with that object ID. The total number of observations that CAR-MHF correctly associated with the track is presented in the column 4. Column 5 is the number of observations CAR-MHF falsely associated (i.e., associated the track with an observation of the wrong fragment). Column 6 is the number of correct associations that CAR-MHF missed. Columns 7–10 are the same as columns 3–6, except that they correspond to the established tracks, that is, filter/smoothen converged and consistent (note that the track number of an established track is assigned upon passing convergence *and* consistency criterion, and thus they do not necessarily correspond to the same track number as its tentative track).

As stated, columns 3–6 of Table 4 show the association performance of the tentative tracks from the CAR-MHF forward-filter-only run. It can be seen that four false tracks were created (meaning that they did not correspond well with any of the true fragments). Track 29 associated with 1754 observations, but none of these were strong associations (maximum β was less than 0.0001, indicating that the uncertainty was very large and associated with observations of many fragments). Tracks 13, 14, and 19 each associated with a few observations, but then lost track of the fragment they were tracking, likely due to the significant initial confusion caused by the large cluster of fragments. When they lost track (i.e., failed to associate to observations of the fragment being tracked), CAR SIOD spawned additional tentative tracks 26, 27, and 28. Table 4 shows that each of those missed a handful of observations, which were at the beginning of the run when tracks 13, 14, and 19 were tracking those fragments (i.e., before tracks 26, 27, and 28 were spawned).

The tentative tracks from the CAR-MHF run were evaluated for convergence, and if converged, they were smoothed. They were

Table 3 25-, 50-, and 100-fragment high-level run results

Case	Start time	Total obs	Compressed obs	Tentative tracks	Established tracks	Recovery rate, %	Average track RMS error, m
25-Fragment	+4 h	34,011	3,954	29	25	100	62
50-Fragment	+4 h	68,283	7,914	99	50	100	67
100-Fragment	+1 day	111,780	12,917	113	99	99	63

Table 4 Measurement association results

Obj ID	Total No. of obs	Tentative (filter only)				Established (smoothed)			
		Track No.	Obs assoc	Missed assoc	False assoc	Track No.	Obs assoc	Missed assoc	False assoc
70000	145	1	146	0	1	3	145	0	0
70001	147	2	152	0	5	1	147	0	0
70002	147	3	150	0	3	4	147	0	0
70003	147	4	150	0	3	2	147	0	0
70004	147	5	147	0	0	5	147	0	0
70005	147	6	147	0	0	6	147	0	0
70006	147	7	147	0	0	7	147	0	0
70007	147	8	147	0	0	8	147	0	0
70008	147	9	147	0	0	9	147	0	0
70009	205	10	205	0	0	10	205	0	0
70010	147	11	158	0	11	11	147	0	0
70011	147	12	154	0	7	12	147	0	0
70012	159	26	152	7	0	23	159	0	0
70013	147	27	139	8	0	24	147	0	0
70014	147	15	150	0	3	13	147	0	0
70015	147	16	148	0	1	14	147	0	0
70016	147	17	147	0	0	15	147	0	0
70017	147	28	140	8	1	25	147	0	0
70018	147	18	154	1	8	16	147	0	0
70019	184	20	186	0	2	17	184	0	0
70020	147	21	147	0	0	18	147	0	0
70021	205	22	210	1	6	19	204	1	0
70022	205	23	206	0	1	20	205	0	0
70023	147	24	148	0	1	21	147	0	0
70024	205	25	206	0	1	22	205	0	0
False track		13	13	—	—				
False track		14	13	—	—				
False track		19	27	—	—				
False track		29	1754	—	—				

filter/smoothen iterated until McReynolds consistency was achieved, at which point they were promoted to established tracks. The established track (number 23) association results are also shown in Table 4 (columns 7–10). The association performance here is nearly perfect, demonstrating the power of the filter/smoothen iteration and track promotion process, which theoretically approaches a batch processor result. CAR-MHF missed only one measurement-to-track association (fragment 70021), and analysis showed that this observation was an outlier. There were no false associations. Using 70012 as an example, as described above, tentative track 26 was not spawned until after the seventh observation of 70012. However, when the track was smoothed back and used to re-initialize the next filter pass, the established track successfully associated with all of the observations of 70012. Because the established tracks are initialized with a smoothed initial condition, they have relatively small uncertainties. During the final filter run before all the estimates were promoted to established tracks, there were no JPDA clusters (i.e., at no point in time did multiple measurements associate with a single track, nor did a single measurement associate with multiple tracks; thus it was a statistically unambiguous measurement-to-track assignment). As seen above, this was not the case for the initial CAR-MHF pass of the data. The CAR-initialized tentative tracks have large initial uncertainties, and thus MH-JPDA was exercised a significant amount during this first pass. That said, the tentative tracks formed were sufficiently accurate to trigger a filter/smoothen iteration that successfully recovered all the fragments.

2. Analysis of Filter/Smoothen Outputs

The second method for evaluation is to evaluate the filter convergence and smoothen consistency behavior. This section reflects the results for fragment 70001, which was represented by tentative track 2 and established track 1. Figure 8 shows the constrained admissible region (and corresponding grid of hypotheses) in range/range-rate space, as well as what the CAR-grid becomes when transformed into orbital elements. Figures 9–15 show plots of the tentative track (filter only) (left) and final filter/smoothen iteration (i.e., established track) (right). Figure 9 shows the CrA/m (coefficient of reflectivity \times area/mass) estimate and uncertainty. The data do not

inform the CrA/m estimate during the first day of the CAR-MHF forward filter pass. On day 2, the value jumps to near its final estimated value and the uncertainty begins to converge; however, the solution is quite noisy. On day 3, the estimate converges on the final value. In the case of the established track (i.e., the final filter/smoothen iteration), it gets initialized near its final value and stays fairly constant while the uncertainty converges throughout the pass. Figures 10 and 11 show the 1-sigma a posteriori position (RIC) and velocity (RIC) uncertainties, respectively. These converge much faster than the CrA/m uncertainties. The established track has much smaller uncertainties (due to the re-initialization) on day 1, but the uncertainties on day 2 and 3 are similar to the tentative track. Figure 12 shows the a priori residuals (innovations along with the 3-sigma uncertainty derived from the innovations covariance). The innovation plots demonstrate that the estimated trajectory predicts future observations within the estimated uncertainty, perhaps the most compelling metric for “real-world” data processing evaluation (i.e., how well the algorithm consistently predicts future behavior is the best that can be done in terms of expected performance). Figure 13 shows the a posteriori residuals. The a posteriori residuals demonstrate unbiased results, with a standard deviation well below the modeled noise. Figures 14 and 15 show the position and velocity McReynolds consistency, respectively. For the tentative track, the McReynolds consistencies are quite poor on day 1 (a McReynolds consistency of less than 3 is considered acceptable). This is due to the large uncertainties (and errors) associated with the CAR SIOD and significant association ambiguities. However, the established track, which has smoothed initial conditions, greatly improved the initial McReynolds consistency on day 1. For the established track, the McReynolds consistency is always less than 3 and almost always less than 2, which indicates excellent consistency.

3. Comparison to Truth

The final evaluation method (only valid for simulated data) is to compare the sets of estimated states with the true states. To evaluate multi-object tracking performance we use a metric that can compare the sets that may be of different cardinality (i.e., number of tracks) and provide an assessment of a mean track precision and accuracy against

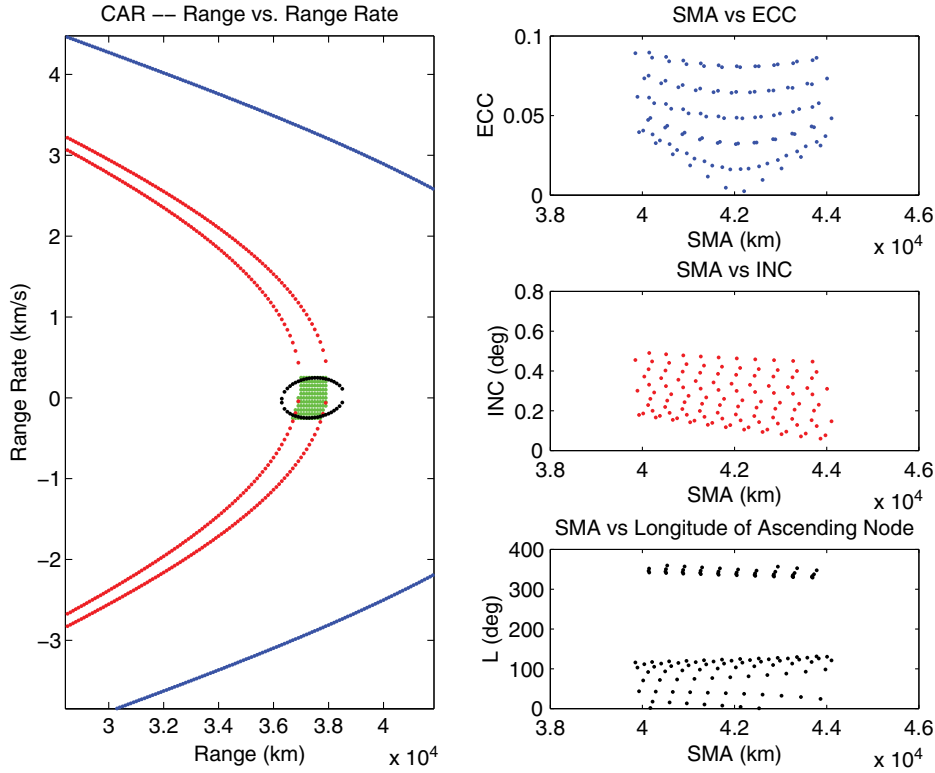


Fig. 8 CAR for fragment 70001.

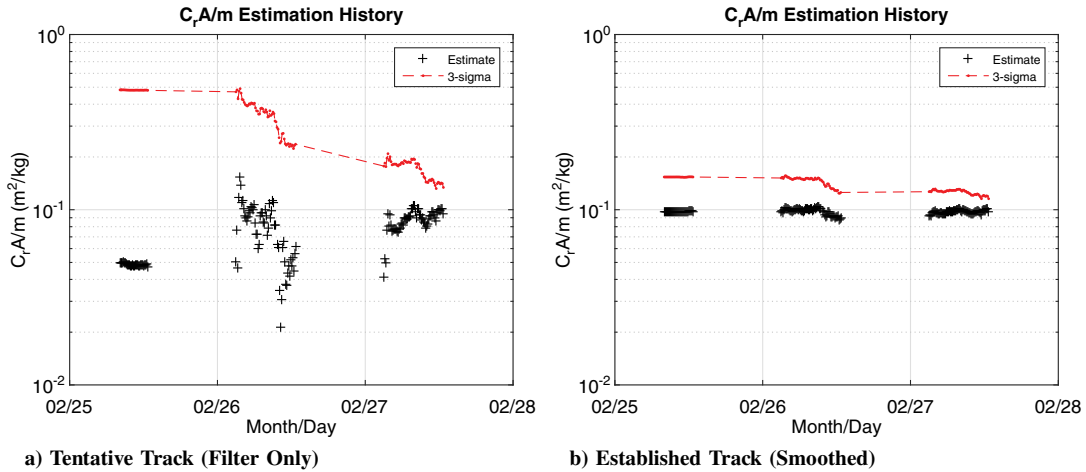


Fig. 9 CrA/m estimate and $1 - \sigma$ uncertainty (note that uncertainty is distance between estimate and 3-sigma line) for fragment 70001.

the truth. To achieve this, the optimal subpattern assignment (OSPA) metric [38] was used. If we define two sets of tracks, $X = \{x_1, \dots, x_m\}$ and $Y = \{y_1, \dots, y_n\}$, the OSPA distance between the sets X and Y is defined as

$$d_p^{(c)}(X, Y) = \left[\frac{1}{n} \left(\min_{\pi \in \Pi_n} \sum_{i=1}^m d^{(c)}(x_i, y_{\pi(i)})^p + c^p(n - m) \right) \right]^{1/p} \quad (27)$$

where $d^{(c)}(x, y) = \min(c, d(x, y))$ is the cutoff distance, with $c > 0$ being the cutoff parameter, $d(x, y)$ is an arbitrary distance metric between x and y , Π_n represents the set of permutations of length m with elements taken from $\{1, 2, \dots, n\}$, and $p \in [1, \infty)$ is the OSPA metric order parameter. For the case where $m > n$ the metric $d_p^{(c)}(Y, X)$ is calculated. The cutoff parameter c determines the relative weighting of the penalties between localization (i.e., state difference) and cardinality errors, whereas the OSPA metric order

parameter p determines the sensitivity to outlier estimates. For the results in this section the parameters $c = 5000$ m and $p = 1$ are used and $d(x, y)$ is the Euclidean distance metric. For each scenario, four sets of estimates were compared with the true states. These sets included tentative (forward-filtered only) tracks and established (smoothed) tracks for both implementations of MH-JPDA (nonparametric MH-JPDA used by Stauch [31] and the new, more efficient parametric MH-JPDA described herein).

Figure 16 displays the results for the 25-fragment scenario. This figure shows the difference between the sets of tentative and established tracks, highlighting the significance of the iterative smoother technique presented. The two implementations of MH-JPDA produced very similar OSPA metrics as expected with only minor differences occurring due to the differences in nonparametric and parametric techniques. After performing the iterative smoothing and refining the initialization, the established tracks were identical for both implementations. For this particular scenario a total of 29 tentative

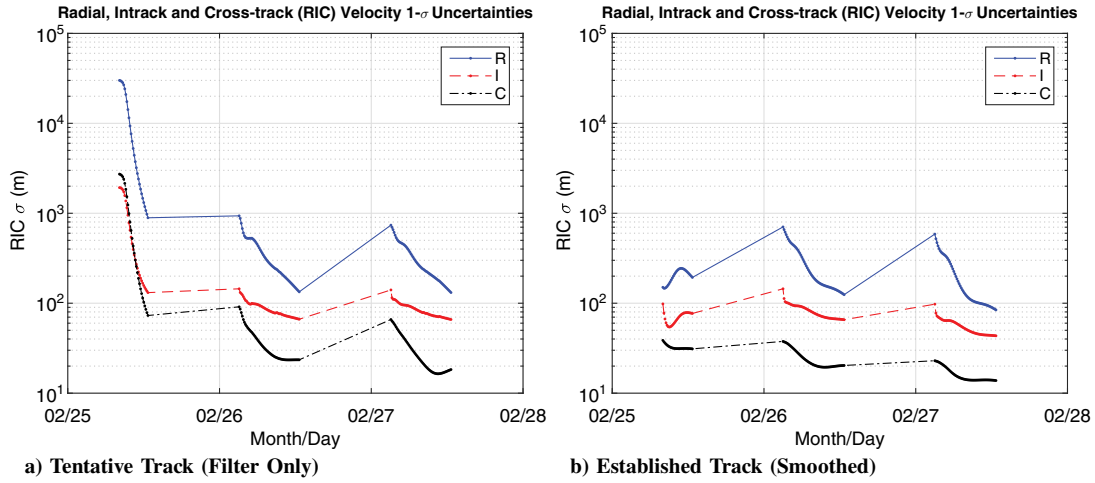


Fig. 10 RIC position $1-\sigma$ uncertainty for fragment 70001.

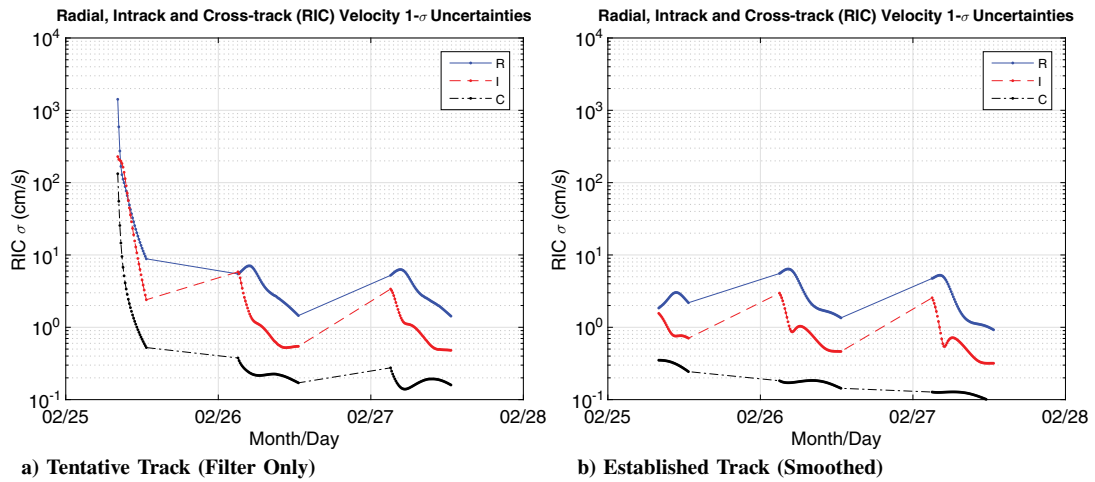


Fig. 11 RIC velocity $1-\sigma$ uncertainty for fragment 70001.

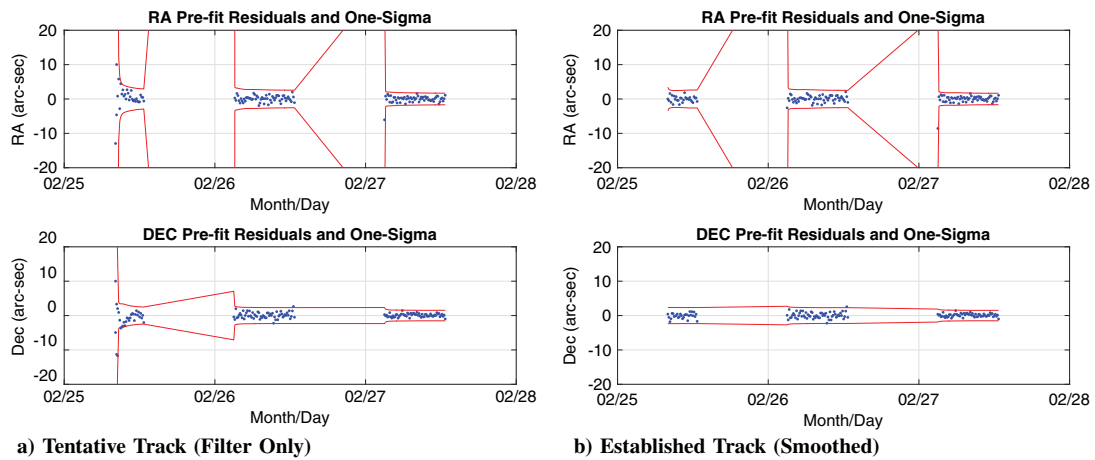


Fig. 12 Innovation (pre-fit residual) and $1-\sigma$ innovation uncertainty for fragment 70001.

tracks were formed, which resulted in 25 established tracks after refinement. The OSPA metric penalizes false tracks and the penalty for the extra tentative (false) tracks can be seen in the figure. This is shown by the difference between the two sets of estimates (tentative and established) after they converged on day 3. It is important to note that even though the two implementations of MH-JPDA gave very similar OSPA metric results, the time to compute the association weights were

drastically different. At the point where most confusion occurred during the scenario (17 objects with 16 measurements), the previous implementation of MH-JPDA spent 22.5 min calculating the result for one particular group of observations, whereas the new efficient implementation reduced that time to 7.4 s (180x speed improvement) (note that larger clusters were found when starting the run immediately after breakup, i.e., 25 objects with 25 measurements,

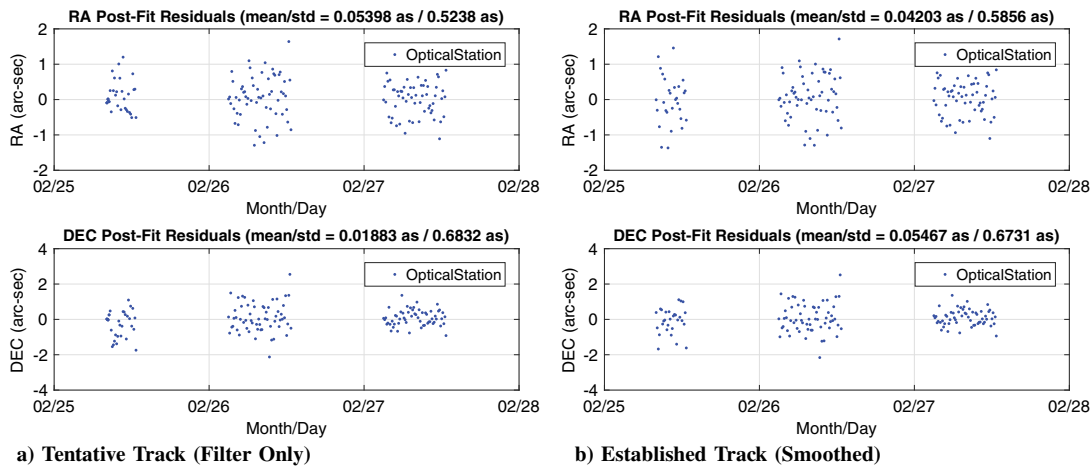


Fig. 13 Post-fit residuals for fragment 70001.

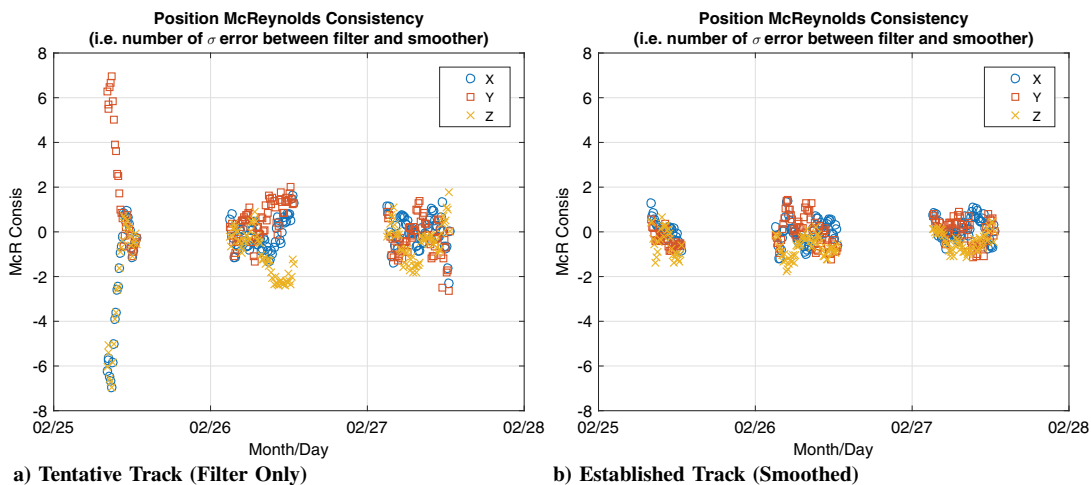


Fig. 14 Position McReynolds consistency for fragment 70001.

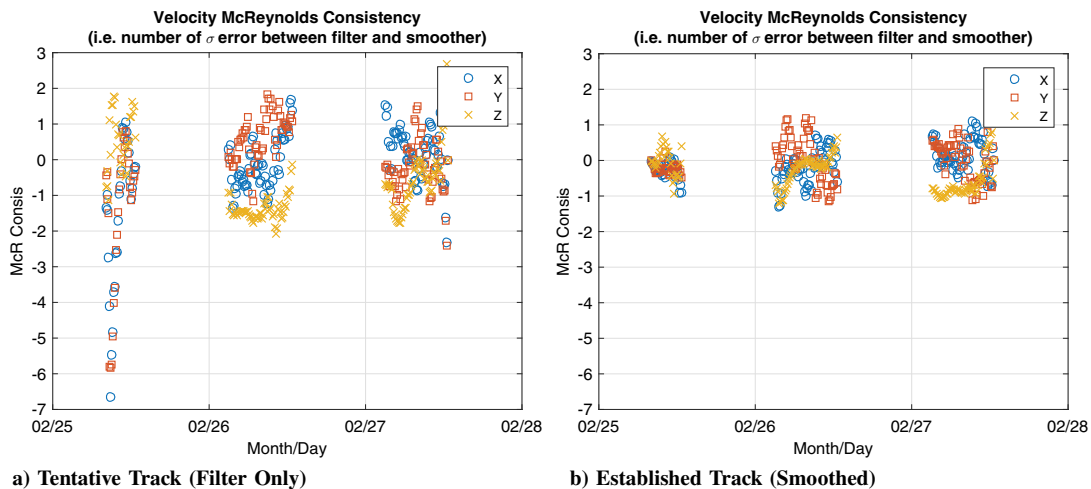


Fig. 15 Velocity McReynolds consistency for fragment 70001.

but these caused out-of-memory errors on our platform). Overall, the time spent to complete the scenario was reduced from 13.5 h to 9.5 min on standard computer hardware. As described in Sec. III.A, this speed improvement is the result of the association calculations being reduced to the single hypothesis case, avoiding the expensive evaluation of joint association events for all combinations of objects, measurements, and hypotheses.

Figures 17 and 18 show the OSPA metric results from the 50- and 100-fragment scenarios, respectively. The established tracks are again identical for both versions of MH-JPDA; however, the tentative tracks show considerable differences. These differences are a result of memory constraints on the hardware used. At certain points in the scenario, if the confusion was too great, the hardware had insufficient memory to calculate the MH-JPDA weights. When this occurred the

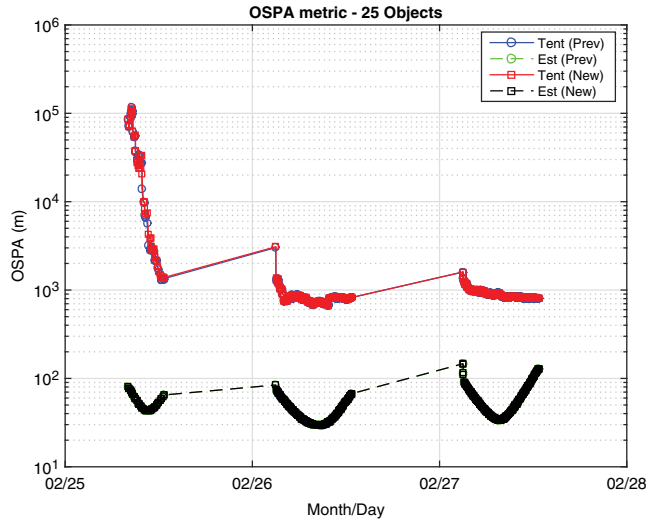


Fig. 16 OSPA metric results from the 25-fragment scenario with tentative and established tracks from two different implementations of the MH-JPDA algorithm.

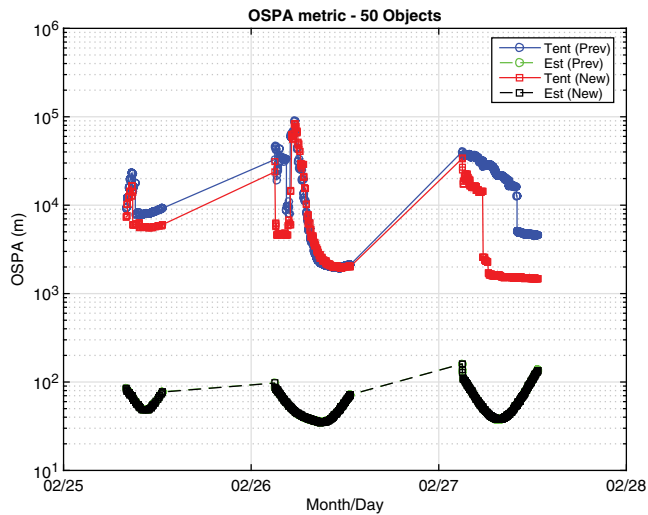


Fig. 17 OSPA metric results from the 50-fragment scenario with tentative and established tracks from two different implementations of the MH-JPDA algorithm.

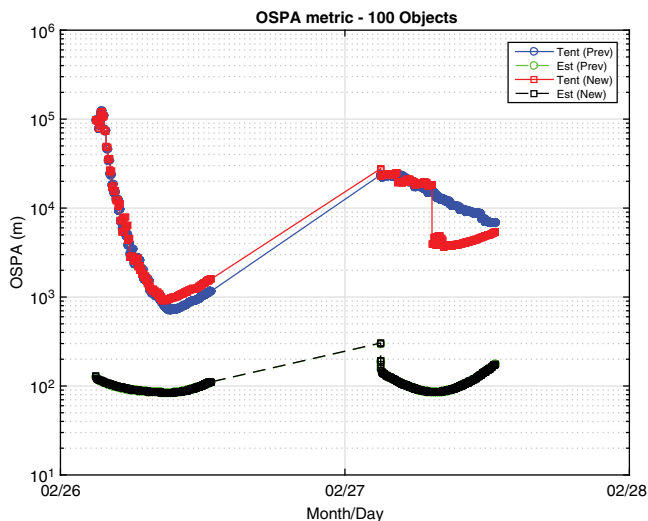


Fig. 18 OSPA metric results from the 100-fragment scenario with tentative and established tracks from two different implementations of the MH-JPDA algorithm.

information from the update was ignored and the algorithm waited for future updates where less confusion was present. Because of the different memory requirements of the MH-JPDA implementations, this condition did not occur at the same time and as a result there were differences between the sets of tentative tracks produced. The new implementation of MH-JPDA was able to reduce the occurrence of such a condition, which resulted in an improved result on day 3 in both the 50- and 100-fragment scenarios. It is understood that, in cases such as this, approximate inference methods such as loopy belief propagation [32] can reduce the computational burden while maintaining accuracy. The figures highlight that even though the tentative estimates were different between the two implementations, the established tracks remained identical. This highlights the importance of the iterative smoothing technique, indicating that the information gained in the forward pass can vary but the same result is achieved after iteratively smoothing.

The average RMS errors of the established tracks when compared with the true states for the 25-, 50-, and 100-fragment scenario were 62, 67, and 63 m, respectively. Given the measurement noise of 2 arc-s, which is equivalent to approximately 400 m at GEO, and no ranging information, this performance is excellent. For tentative tracks, although initial errors are relatively large (100+ km), the uncertainties are realistic, allowing for proper data association. Additionally, the advantage of initializing the state with the smoothed initial condition is demonstrated given the significantly smaller a posteriori errors.

VI. Conclusions

The application of multiple hypothesis joint probabilistic data association (MH-JPDA), combined with an RTS UKF smoother, for simultaneous tracking of multiple space objects has been presented and demonstrated within Constrained Admissible Region, Multiple Hypothesis Filter (CAR-MHF) to track a simulated geosynchronous Earth orbit breakup scenario. This method has the dual advantage of a sequential, real-time functionality and a refined capability equivalent to a batch processor or differential corrector. In certain situations, this method could be preferable to a multiple hypothesis tracker (MHT) in that statistical initial orbit determination (SIOD) combined with an MH-JPDAF enables immediate track initiation and real-time sequential processing (i.e., there is no need to wait for “ n ” tracks to exist in order for an answer to be provided; CAR-MHF provides an answer as soon as any data are made available). Additionally, it is well established that JPDA is superior to nearest neighbor, particularly applied to closely spaced objects and/or large uncertainties (both of which apply for a breakup scenario).

The CAR SIOD method results in large initial errors (due to the limited information content of a short angles-only tracklet), but the CAR-generated track uncertainties are realistic, and thus future measurements are properly associated to the track. These large initial uncertainties cause overlap and observation association confusion, and thus MH-JPDA is needed. The results show that MH-JPDA is able to converge quickly on the trajectory in spite of this initial ambiguity. Track refinement via an UKF RTS smoother significantly reduces the track errors and allows for an established track promotion strategy. This approach directly supports an autonomous and robust catalog development and subsequent maintenance capability. Additionally, the smoother refinement process approaches the performance of a batch processor with unique detection-to-object assignments. CAR-MHF with MH-JPDA and smoothing is demonstrated to converge to an accuracy better than the measurement noise. This approach can account for and estimate model characteristics (e.g., area-to-mass ratio), beneficial for prediction accuracy and association performance. The optimal subpattern assignment results demonstrate the method’s ability to achieve accurate trajectories, as well as recover the correct number of objects (i.e., cardinality).

The efficient parametric MH-JPDA algorithm presented here generates the same result, in both precision and accuracy, as the previous implementation (which implemented nonparametric JPDA) with more than two orders of magnitude speed improvement.

Acknowledgments

The work was funded under a contract with the Air Force Research Lab, Kirtland Air Force Base, Albuquerque, NM. We would like to thank Dr. Ryan Weisman for providing a meaningful and valuable review and critique of this paper. We would also like to thank Dr. Kyle DeMars, who supplied many of the CAR- and MHF-related algorithms that were incorporated into the foundations of CAR-MHF. We are especially appreciative of Dr. Tom Kececy and Dr. Jason Williams. Dr. Kececy was a major contributor to the development of the CAR-MHF code (and continues to contribute). Dr. Williams derived the simplification of parametric MH-JPDA (shown in Sec. III) that allows for a substantial speed improvement.

References

- [1] "Joint Doctrine for Space Operations," U.S. Department of Defense, Joint Publication 3-14, May 2013.
- [2] Sabol, C., Segerman, A., Hoskins, A., Little, B., Schumacher, P., and Coffey, S., "Search and Determine Integrated Environment (Sadie) for Space Situational Awareness," *Proceedings from the AMOS Technical Conference*, Maui Economic Development Board, Kihei, HI, 2012.
- [3] Sabol, C., Hill, K., Alfriend, K., and Sukut, T., "Nonlinear Effects in the Correlation of Tracks and Covariance Propagation," *Acta Astronautica*, Vol. 84, March–April 2013, pp. 69–80. doi:10.1016/j.actaastro.2012.08.023
- [4] Escobal, P. R., *Methods of Orbit Determination*, Krieger Publishing Company, Malabar, FL, 1965.
- [5] Gooding, R. H., "A New Procedure for Orbit Determination Based on Three Line of Sight (Angles Only)," Defense Research Agency Tech. Rept. 93004, Farnborough, U.K., 2004.
- [6] DeMars, K. J., Jah, M. K., and Schumacher, P. W., "Initial Orbit Determination Using Short-Arc Angle and Angle Rate Data," *IEEE Transactions on Aerospace and Electronic Systems*, Vol. 48, No. 3, 2012, pp. 2628–2637. doi:10.1109/TAES.2012.6237613
- [7] DeMars, K. J., and Jah, M. K., "Probabilistic Initial Orbit Determination Using Gaussian Mixture Models," *Journal of Guidance, Control, and Dynamics*, Vol. 36, No. 5, 2013, pp. 1324–1335. doi:10.2514/1.59844
- [8] Blackmann, S., and Popoli, R., *Design and Analysis of Modern Tracking Systems*, Artech House, 1999.
- [9] Bar-Shalom, Y., and Li, X. R., *Multitarget-Multisensor Tracking: Principles and Techniques*, YBS Publishing, Storrs, CT, 1995.
- [10] Reid, D., "An Algorithm for Tracking Multiple Targets," *IEEE Transactions on Automatic Control*, Vol. 21, No. 1, Feb. 1976, pp. 101–104.
- [11] Blackman, S., "Multiple Hypothesis Tracking for Multiple Target Tracking," *IEEE A&E Systems Magazine*, Vol. 19, No. 1, pp. 5–18, Jan. 2004. doi:10.1109/MAES.2004.1263228
- [12] Mahler, R. P. S., *Statistical Multisource-Multitarget Information Fusion*, Artech House, Norwood, MA, 2007.
- [13] Williams, J. L., "Experiments with Graphical Model Implementations of Multiple Target Multiple Bernoulli Filters," *Proceedings of the 7th International Conference on Intelligent Sensors, Sensor Networks and Information Processing*, IEEE Publ., Piscataway, NJ, Dec. 2011, pp. 532–537. doi:10.1109/ISSNIP.2011.6146620
- [14] Reuter, S., Vo, B.-T., Vo, V.-N., and Dietmayer, K., "The Labeled Multi-Bernoulli Filter," *IEEE Transactions on Signal Processing*, Vol. 62, No. 12, June 2014, pp. 3246–3260. doi:10.1109/TSP.2014.2323064
- [15] Rauch, H. E., Tung, F., and Striebel, C. T., "Maximum Likelihood Estimation for Linear Dynamic Systems," *AIAA Journal*, Vol. 3, No. 8, Aug. 1965, pp. 1445–1450. doi:10.2514/3.3166
- [16] Psiaki, M. L., and Wada, M., "Derivation and Simulation Testing of a Sigma-Points Smoother," *Journal of Guidance, Control, and Dynamics*, Vol. 30, No. 1, 2007, pp. 78–86. doi:10.2514/1.22875
- [17] Sarkka, S., "Unscented Rauch-Tung-Striebel Smoother," *IEEE Transactions on Automatic Control*, Vol. 53, No. 3, 2008, pp. 845–849. doi:10.1109/TAC.2008.919531
- [18] McReynolds, S. R., "Editing Data Using Sequential Smoothing Techniques for Discrete Systems," *Proceedings of the AIAA/AAS Astrodynamics Conference*, AIAA Paper 1984-2053, Aug. 1984.
- [19] Kececy, T., Jah, M. K., Baldwin, J., and Stauch, J., "Hi Area-to-Mass Ratio Object Population Assessment from Data/Track Association," *Acta Astronautica*, Vol. 96, March–April 2014, pp. 166–174. doi:10.1016/j.actaastro.2013.11.037
- [20] Kececy, T., Shoemaker, M., and Jah, M., "Application of the Constrained Admissible Region Multiple Hypothesis Filter to Initial Orbit Determination of a Break-Up," *6th European Conference on Space Debris*, Astrophysics Data System, April 2013, pp. 22–25.
- [21] Milani, A., Gronchi, G. F., Vitturi, M., and Knezevic, Z., "Orbit Determination with Very Short Arcs. I Admissible Regions," *Celestial Mechanics and Dynamical Astronomy*, Vol. 90, Nos. 1–2, July 2004, pp. 57–85. doi:10.1007/s10569-004-6593-5
- [22] Julier, S. J., and Uhlmann, J. K., "Unscented Filtering and Nonlinear Estimation," *Proceedings of the IEEE*, Vol. 93, No. 3, March 2004.
- [23] Bar-Shalom, Y., and Fortmann, T. E., *Tracking and Data Association*, Academic Press, Cambridge, MA, 1988.
- [24] DeMars, K. J., Bishop, R. H., and Jah, M. K., "Entropy-Based Approach for Uncertainty Propagation of Nonlinear Dynamical Systems," *Journal of Guidance, Control, and Dynamics*, Vol. 36, No. 4, May 2013, pp. 1047–1057. doi:10.2514/1.58987
- [25] Julier, S. J., Uhlmann, J. K., and Durrant-Whyte, H. F., "A New Method for the Nonlinear Transformation of Means and Covariances in Filters and Estimators," *IEEE Transactions on Automatic Control*, Vol. 45, No. 3, March 2000, pp. 477–482. doi:10.1109/9.847726
- [26] Van der Merwe, R., "Sigma-Point Kalman Filters for Probabilistic Inference in Dynamic State-Space Models," Ph.D. Dissertation, Oregon Health and Science Univ., April 2004.
- [27] Weisman, R. M., and Jah, M. K., "Uncertainty Quantification for Angles-Only Initial Orbit Determination," *AAS/AIAA Spaceflight Mechanics Meeting*, AAS Paper 14-434, Sante Fe, NM, Jan. 2014.
- [28] Bar-Shalom, Y., and Tse, E., "Tracking in a Cluttered Environment with Probabilistic Data Association," *Automatica*, Vol. 11, No. 5, Sept. 1975, pp. 451–460. doi:10.1016/0005-1098(75)90021-7
- [29] Fortmann, T. E., Bar-Shalom, Y., and Scheffe, M., "Sonar Tracking of Multiple Targets Using Joint Probabilistic Data Association," *IEEE Journal of Oceanic Engineering*, Vol. 8, No. 3, July 1983, pp. 173–184. doi:10.1109/JOE.1983.1145560
- [30] Bar-Shalom, Y., *Multitarget-Multisensor Tracking: Applications and Advances*, Vol. III, Artech House Inc., Norwood, MA, 2000.
- [31] Stauch, J., Jah, M., Baldwin, J., Kececy, T., and Hill, K., "Mutual Application of Joint Probabilistic Data Association, Filtering, and Smoothing Techniques for Robust Multiple Space Object Tracking," *AIAA/AAS Astrodynamics Specialist Conference*, AIAA Paper 2014-4365, Aug. 2014.
- [32] Ruten, M., Williams, J., Gordon, N., Stauch, J., Baldwin, J., and Jah, M., "A Comparison of JPDA and Belief Propagation for Data Association in SSA," *Proceedings from the AMOS Technical Conference*, Maui Economic Development Board, Kihei, HI, Sept. 2014.
- [33] Chen, B., and Tugnait, J. K., "Tracking of Multiple Maneuvering Targets in Clutter Using IMM/JPDA Filtering and Fixed-Lag Smoothing," *Automatica*, Vol. 37, No. 2, Feb. 2001, pp. 239–249. doi:10.1016/S0005-1098(00)00158-8
- [34] Williams, J. L., and Lau, R. A., "A Structured Mean Field Approach for Existence-Based Multiple Target Tracking," *Proceedings of the 19th International Conference on Information Fusion*, IEEE Publ., Piscataway, NJ, July 2016, <http://ieeexplore.ieee.org>.
- [35] Blom, H. A. P., Bloem, E. A., and Musicki, D., "Jipda*: Automatic Target Tracking Avoiding Track Coalasence," *IEEE Transactions on Aerospace and Electronic Systems*, Vol. 51, No. 2, April 2015, pp. 962–974. doi:10.1109/TAES.2014.130327
- [36] Wetterer, C., Linares, R., Crassidis, J., Kececy, T., Ziebart, M., Jah, M., and Cefola, P., "Refining Space Object Radiation Pressure Modeling with Bidirectional Reflectance Distribution Functions," *Journal of Guidance, Control, and Dynamics*, Vol. 37, No. 1, 2014, pp. 185–196. doi:10.2514/1.60577
- [37] Pines, S., "Uniform Representation of the Gravitational Potential and Its Derivatives," *AIAA Journal*, Vol. 11, No. 11, Nov. 1973, pp. 1508–1511. doi:10.2514/3.50619
- [38] Schuhmacher, D., Vo, B.-T., and Vo, B.-N., "A Consistent Metric for Performance Evaluation of Multi-Object Filters," *IEEE Transactions on Signal Processing*, Vol. 56, No. 8, Aug. 2008, pp. 3447–3457. doi:10.1109/TSP.2008.920469